PHYSICAL REVIEW D **91,** 063508 (2015)

Quantitative study of the AMS-02 electron/positron spectra: Implications for pulsars and dark matter properties

Su-Jie Lin, Qiang Yuan, and Xiao-Jun Bi

Key Laboratory of Particle Astrophysics, Institute of High Energy Physics, Chinese Academy of Science, Beijing 100049, People's Republic of China

(Received 3 December 2014; published 5 March 2015)

The Alpha Magnetic Spectrometer (AMS-02) has just published the unprecedentedly precise measurement of the cosmic electron and positron spectra. In this paper, we try to give a quantitative study on the AMS-02 results by a global fitting to the electron and positron spectra, together with the updated positron fraction data. The Markov chain Monte Carlo algorithm is adopted to do the fitting. The primary electron spectrum and the parameters for pulsars or dark matter that contribute extra positrons are determined simultaneously. We find that there is a hardening of the primary electron spectrum at ∼60 GeV. With such a new feature at the background spectrum, both the pulsars and dark matter can explain the AMS-02 results very well. The dark matter scenario shows a drop at the positron fraction at ∼300 GeV but suffers very strong constraints from Fermi γ-ray observations. The fitting results also suggest that the propagation model with convection may be more favored by the lepton data than the reacceleration model.

DOI: 10.1103/PhysRevD.91.063508 PACS numbers: 95.35.+d

I. INTRODUCTION

There has been much progress in the measurements of the cosmic ray (CR) lepton fluxes in recent years. Satellite experiments such as the Payload for Antimatter Matter Exploration and Light-Nuclei Astrophysics (PAMELA) and the Fermi Large Area Telescope (Fermi-LAT), as well as the balloon-borne detector such as the Advanced Thin Ionization Calorimeter (ATIC) and the ground-based Cherenkov telescopes like the High Energy Stereoscopic System (HESS) and the Major Atmospheric Gamma-Ray Imaging Cherenkov Telescopes (MAGIC), have improved the uncertainties of the measurements from an order of magnitude down to several tens of percents [1–7]. The space station experiment Alpha Magnetic Spectrometer (AMS-02), launched in May 2011, further improved the measurement precision of the CR fluxes by an order of magnitude due to larger exposure and much better control of the systematics [8]. With the AMS-02 result, we could perform the study of CRs in a more quantitative way instead of the qualitative studies [9–12].

The most interesting features found in the CR leptons are the excess of the positrons compared with the secondary background expectation from CR nuclei interaction with the interstellar medium (ISM) [1,8,13,14]. Combining with the electron (or total electron/positron) spectra [2,3,5–7] implies that there should be extra sources emitting electron-positron pairs. The proposed models of the extra sources include the astrophysical sources such as pulsars [15–19], interaction occurring around the CR acceleration sources [20–22], and the dark matter (DM) annihilation/decay [23–28]. One can refer to the reviews for a detailed description of the relevant models to explain the electron/positron excesses [29–33].

Given that the data are more abundant and precise, we developed a global fitting tool that employs a Markov chain Monte Carlo (MCMC) [34] method to sample the high-dimensional parameter space of the CR propagation and injection [35,36]. When applied in the study of the electron/positron excesses, such a global fitting method can fit both the background and the extra source parameters simultaneously and avoid the bias of choosing the background parameters. This approach definitely makes sense on the quantitative level, despite that there are still uncertainties from various kinds of model configurations such as the CR propagation and the solar modulation [37]. It is expected that, with better understandings of those issues based on more and better data from AMS-02, the global fitting method may be more powerful to probe the underlying physical nature of the CRs.

One potential problem of the previous studies about the CR leptons is the systematical uncertainties among different detectors. As shown by the preliminary data of AMS-02 presented at the 2013 International Cosmic Ray Conference [38], many kinds of measurements showed differences compared to previous measurements. Furthermore, the data-taking periods of various experiments are also different, and the solar modulation effect will be different. It is no longer a problem after the most recent data release about the positron and electron fluxes by AMS-02 [39–41]. In this work, we adopt the AMS-02 data about the positron fraction, positron plus electron flux, positron flux, and the electron flux to study the injection properties of the backgrounds and the extra sources of the CR leptons.

This paper is organized as follows. We first give a description of our fitting process in Sec. II. The propagation of CRs in the Galaxy is introduced in Sec. III. The

assumptions and parametrization of the backgrounds and extra sources of electrons/positrons are described in Secs. IV and V. The fitting results in different models are given in Sec. VI. We give some discussions about the results in Sec. VI and conclude in Sec. VIII.

II. SCHEME OF THE GLOBAL FITTING

The scheme of the global fitting follows our previous study of the AMS-02 positron fraction results [9]. The model consists of the primary electrons, secondary electrons/positrons and electrons/positrons from the extra sources such as pulsar-like astrophysical sources or the DM. We adopt a set of parameters $\vec{\theta}$ to describe the model. These parameters will be defined in the next sections. Once the parameters are given, we can calculate the propagation of the CRs in the Milky Way. The production and propagation of secondary positrons/electrons will also be calculated at the same time. Then, we compare the predicted spectra with the AMS-02 data and evaluate the model by minimizing the χ^2.

The MCMC technique is used to derive the posterior probability distributions of the parameters from the observational data. According to the Bayes theorem, the posterior probability of a set of parameters $\vec{\theta}$ in light of the observational data is $\mathcal{P}(\vec{\theta}|D) \propto \mathcal{P}(D|\vec{\theta})\mathcal{P}(\vec{\theta})$, where $\mathcal{P}(D|\vec{\theta}) = \mathcal{L}(\vec{\theta}) \propto \exp(-\chi^2(\vec{\theta})/2)$ is the likelihood function of model $\vec{\theta}$ for the data and $\mathcal{P}(\vec{\theta})$ is the prior probability of the model parameters before the current observations. In this work, we adopt flat (constant) prior probabilities of all the model parameters in specified ranges (some of them are logarithmical; see the details in the tables below).

We adopt the Metropolis–Hastings algorithm to generate the Markov chains from the unknown target distribution. The Metropolis–Hastings algorithm adopts a propose-and-accept process, in which the acceptance or rejection of a proposed point depends on the probability ratio between this point and the former one, to generate the chains. Such a sampling method can still work efficiently when the dimension of the parameter space is high.

The propagation model parameters will be first determined by fitting the boron-to-carbon (B/C) ratio and unstable-to-stable beryllium (^{10}Be/^{9}Be) ratio data (see a more detailed description in Sec. III). The propagation parameters are then fixed to be the best-fitting values when fitting the lepton data. The proton injection spectrum is also determined by fitting the AMS-02 data [38]. Therefore, in the fitting process, the parameter space $\vec{\theta}$ includes only the parameters of the lepton sector.

The global fitting gives us information of the background and properties of the extra sources at the same time. Therefore, results on the astrophysical sources and DM are not biased due to the choice of background. The parameters for DM given in the work can be taken as the starting point for the future model building. The results for pulsars can also be a guideline for pulsar model study although the case for pulsars is more complicated as each pulsar may have different properties. What we get may indicate the property of a nearby pulsar that gives a dominant contribution to the positron excess.

III. PROPAGATION OF COSMIC RAYS IN THE GALAXY

Galactic CR particles diffuse in the Galaxy after being accelerated, suffering from the fragmentation and energy loss in the ISM and/or the interstellar radiation field and magnetic field, decay, and possible reacceleration or convection. Denoting the density of CRs per unit momentum interval as ψ, the propagation can be described by the propagation equation

$$\frac{\partial \psi}{\partial t} = Q(\mathbf{x}, p) + \nabla \cdot (D_{xx}\nabla\psi - \mathbf{V}_c\psi) + \frac{\partial}{\partial p} p^2 D_{pp} \frac{\partial}{\partial p}\frac{1}{p^2}\psi - \frac{\partial}{\partial p}\left[\dot{p}\psi - \frac{p}{3}(\nabla \cdot \mathbf{V}_c\psi)\right] - \frac{\psi}{\tau_f} - \frac{\psi}{\tau_r}, \quad (1)$$

where $Q(\mathbf{x}, p)$ is the source distribution, D_{xx} is the spatial diffusion coefficient, $\mathbf{V}_c$ is the convection velocity, D_{pp} is diffusion coefficient in the momentum space, and τ_f and τ_r are the characteristic time scales used to describe the fragmentation and radioactive decay. The convection velocity $\mathbf{V}_c$ is generally assumed to linearly depend on the distance away from the Galaxy disk. The diffusion coefficient can be parametrized as $D_{xx} = D_0\beta(R/R_0)^\delta$, where β is the velocity of the particle in the unit of light speed c and $R \equiv pc/Ze$ is the rigidity. The reacceleration effect is described with the diffusion in momentum space. Considering the scenario in which the CR particles are reaccelerated by colliding with the interstellar random weak hydrodynamic waves, the relation between the spatial diffusion coefficient D_{xx} and the momentum diffusion coefficient D_{pp} can be expressed as [42,43]

TABLE I. The mean values and 1σ uncertainties of the propagation parameters derived through fitting the B/C and ^{10}Be/^{9}Be ratios. In the DC scenario, δ is set to be zero when R is below R_0.

		DR	DC
D_0	(10^{28} cm^2 s^{-1})	6.58 ± 1.27	1.95 ± 0.50
δ		0.333 ± 0.011	0.510 ± 0.034
R_0	(GV)	4	4.71 ± 0.8
v_A	(km s^{-1})	37.8 ± 2.7	⋯
$\mathrm{d}V/\mathrm{d}z$	(km s^{-1} kpc^{-1})	⋯	4.2 ± 3.2
z_h	(kpc)	4.7 ± 1.0	2.5 ± 0.7
ϕ	(MV)	326 ± 36	182 ± 25

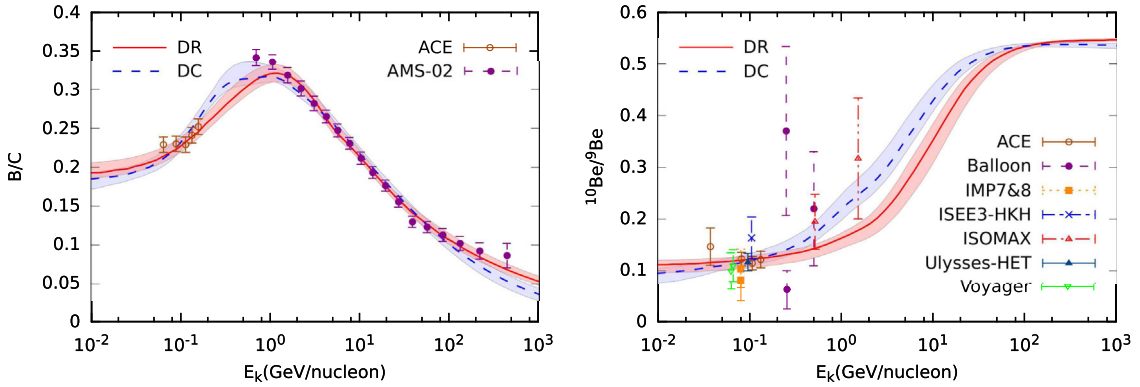

FIG. 1 (color online). The B/C ratio (left) and ^{10}Be/^{9}Be ratio (right) for the corresponding parameters shown in Table I, compared with the data. The bands show the 95% confidence ranges. The B/C data are from AMS-02 [38] and ACE [46], and the ^{10}Be/^{9}Be data are from experiments ACE [47], Balloon [48–50], IMP7&8 [51], ISEE3-HKH [52], ISOMAX [53], Ulysses-HET [54], and Voyager [55].

$$D_{pp}D_{xx} = \frac{4p^2v_A^2}{3\delta(4-\delta^2)(4-\delta)\omega}, \tag{2}$$

where v_A is the Alfven velocity and the parameter ω is used to characterize the level of the interstellar turbulence. Since only v_A^2/ω is relevant, we adopt $\omega = 1$ and refer v_A to characterize the reacceleration. Free escape is assumed at the boundaries, R_h and z_h, for cylindrical geometry.

The secondary-to-primary ratios of nuclei are almost independent of the injection spectrum. They are always employed to constrain the propagation parameters in Eq. (1). Generally used are the B/C and ^{10}Be/^{9}Be ratios. The B/C ratio is sensitive to the average path the CR particles go through between the source and the observer, which correlate positively with both D_{xx} and the diffusion halo size z_h. The ^{10}Be/^{9}Be ratio is sensitive to probe the resident time of particles in the Galaxy, which correlate positively with z_h but negatively with D_{xx}. Therefore, combining these two ratios, the main propagation properties can be fixed.

The major parameters to describe the propagation are $(D_0, \delta, v_A, \mathrm{d}V/\mathrm{d}z, z_h)$. Since there are degeneracies between the models with reacceleration and convection effects, and the current data of B/C and ^{10}Be/^{9}Be are not effective enough to distinguish them, we adopt two distinct scenarios as benchmark models of the propagation. They are referred to as the diffusion reacceleration (DR) model and diffusion convection (DC) model, respectively.

The public numerical tool, GALPROP version 54.1.984[1] [44,45], is adopted to calculate the propagation of CR particles. We employ the B/C ratio data from AMS-02 [38] and ACE [46] and the ^{10}Be/^{9}Be ratio data from experiments ACE [47], Balloon [48–50], IMP7&8 [51], ISEE3-HKH [52], ISOMAX [53], Ulysses-HET [54], and Voyager [55] to constrain the propagation parameters. The MCMC method is adopted to fit the B/C ratio and ^{10}Be/^{9}Be ratio data. To reproduce the low-energy B/C ratio data, a broken power law, in which δ is zero when R is below R_0, is adopted for D_{xx} in the DC scenario [56]. To describe the propagation of CR particles in the Solar System, we adopt the force-field approximation [57], which contains only one free parameter, the so-called solar modulation potential ϕ. The mean values and 1σ errors of the propagation parameters for DR and DC scenarios are shown in Table I. Figure 1 shows the fitting results of B/C (left) and ^{10}Be/^{9}Be (right) ratios within 2σ confidence level, compared with the observational data.

[1]Available at http://galprop.stanford.edu/.

IV. PARAMETERS FOR THE BACKGROUND e^+ AND e^- SPECTRA

Electrons are also expected to be accelerated during the acceleration of CR nuclei at the sources, e.g., supernova remnants (SNRs). During the propagation, the inelastic collision between the nuclei and the ISM will produce secondary electrons and positrons. These components consist of the background contribution of electrons and positrons. Such a picture is supported by the observations

TABLE II. The nucleon injection parameters derived through fitting the proton data of AMS-02. A single power law is enough to fit the data in the DC scenario.

	Prior range	DR	DC
ν_1	[1.0, 4.0]	1.811 ± 0.021	2.336 ± 0.004
ν_2	[1.0, 4.0]	2.402 ± 0.005	2.336 ± 0.004
R_{br}^p (GV)	[8.0, 15.0]	12.88 ± 0.263	10.00
A_p[a]	[3.0, 6.0]	4.613 ± 0.027	4.783 ± 0.026
ϕ_p (MV)	[50, 1500]	517.8 ± 37.8	505.9 ± 13.1

[a]Postpropagated normalization flux of protons at 100 GeV in units of 10^{-9} cm^{-2} s^{-1} sr^{-1} MeV^{-1}.

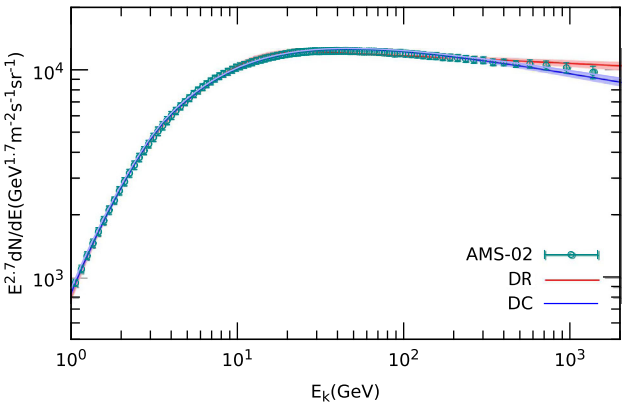

FIG. 2 (color online). The fluxes of protons for the corresponding parameter shown in Table II, compared with the preliminary data from AMS-02 [38]. The bands delimit the regions of the 95% confidence level.

of the secondary-to-primary ratio of nuclei as well as the diffuse γ-ray emission [58,59].

The spatial distribution of the injected CR particles is assumed to follow the SNR distribution

$$f(r,z) = \left(\frac{r}{r_\odot}\right)^a \exp\left(-b\cdot\frac{r-r_\odot}{r_\odot}\right)\exp\left(-\frac{|z|}{z_s}\right), \quad (3)$$

where $r_\odot = 8.5$ kpc is the distance from the Sun to the Galactic center and $z_s \approx 0.2$ kpc is the characteristic height of Galactic disk. The two parameters a and b are chosen to be 1.25 and 3.56, following Ref. [60], and are adjusted to fit the γ-ray gradient. The injection spectra of all kinds of nuclei are assumed to be a broken power law form,

$$q_{\rm i} = N_{\rm i} \times \begin{cases} \left(\frac{R}{R^{\rm p}_{\rm br}}\right)^{-\nu_1} & R \le R^{\rm p}_{\rm br} \\ \left(\frac{R}{R^{\rm p}_{\rm br}}\right)^{-\nu_2} & R > R^{\rm p}_{\rm br} \end{cases}, \quad (4)$$

where i denotes species of the nuclei, R is the rigidity of the particle, and $N_{\rm i}$ is the normalization constant proportional to the relative abundance of the corresponding nuclei. The injection is simply assumed to be stable, which is an effective approximation if the production rate of SNRs is high enough. Therefore, the injection source function can then be written as $Q_{\rm i}(\mathbf{x}, p) = f(r,z)q_{\rm i}(p)$.

TABLE III. Fitting results of pulsar model with one break in the e^- injection spectrum.

		DR		DC	
	Prior range	Best	Mean	Best	Mean
$\log(A_e)$[a]	$[-10.5, -7.5]$	-8.812	-8.813 ± 0.002	-8.897	-8.897 ± 0.002
γ_1	[1.0, 3.0]	1.896	1.878 ± 0.025	2.268	2.264 ± 0.02
γ_2	[1.5, 4.0]	2.874	2.872 ± 0.005	2.725	2.726 ± 0.005
$\log(R^e_{\rm br}/{\rm MV})$	[3.0, 6.0]	3.697	3.68 ± 0.025	3.812	3.808 ± 0.014
$\log(A_{\rm psr})$[b]	$[-35.0, -20.0]$	-25.99	-25.91 ± 0.21	-25.31	-25.35 ± 0.12
α	[1.0, 2.4]	1.749	1.763 ± 0.039	1.859	1.851 ± 0.022
$\log(R_{\rm c}/{\rm MeV})$	[4.0, 10.0]	9.621	8.88 ± 0.7	9.168	8.782 ± 0.77
c_{e^+}	[0.25, 4.0]	2.63	2.599 ± 0.057	1.204	1.216 ± 0.033
ϕ/MV	[100, 1500]	1410.0	1402.0 ± 13.0	562.1	565.9 ± 12.0

[a]Postpropagated normalization flux of e^- at 25 GeV in units of $\rm cm^{-2}\,s^{-1}\,sr^{-1}\,MeV^{-1}$.
[b]Prepropagated normalization of pulsar injection at 1 MeV in units of $\rm cm^{-3}\,s^{-1}\,MeV^{-1}$.

TABLE IV. Fitting results of the DM annihilation scenario in the $\mu^+\mu^-$ channel with one break in the e^- injection spectrum.

		DR		DC	
	Prior range	Best	Mean	Best	Mean
$\log(A_e)$[a]	$[-10.5, -7.5]$	-8.801	-8.801 ± 0.001	-8.872	-8.872 ± 0.002
γ_1	[1.0, 3.0]	1.925	1.913 ± 0.018	2.303	2.301 ± 0.037
γ_2	[1.5, 4.0]	2.9	2.9 ± 0.003	2.79	2.789 ± 0.004
$\log(R^e_{\rm br}/{\rm MV})$	[3.0, 6.0]	3.706	3.692 ± 0.019	3.702	3.704 ± 0.016
$\log(m_\chi/{\rm GeV})$	[0.0, 7.0]	3.179	3.178 ± 0.066	2.654	2.65 ± 0.018
$\log(\langle\sigma v\rangle)$[b]	$[-28.0, -18.0]$	-22.85	-22.86 ± 0.12	-23.42	-23.43 ± 0.029
c_{e^+}	[0.25, 4.0]	2.997	2.994 ± 0.019	1.775	1.771 ± 0.014
ϕ/MV	[100, 1500]	1488.0	1488.0 ± 6.7	748.2	744.8 ± 7.9

[a]Postpropagated normalization flux of e^- at 25 GeV in units of $\rm cm^{-2}\,s^{-1}\,sr^{-1}\,MeV^{-1}$.
[b]In units of $\rm cm^3\,s^{-1}$.

TABLE V. Fitting results of the DM annihilation scenario in the $\tau^+\tau^-$ channel with one break in the e^- injection spectrum.

		DR		DC	
	Prior range	Best	Mean	Best	Mean
$\log(A_e)$[a]	$[-10.5, -7.5]$	-8.803	-8.803 ± 0.002	-8.883	-8.882 ± 0.002
γ_1	[1.0, 3.0]	1.915	1.909 ± 0.019	2.299	2.295 ± 0.031
γ_2	[1.5, 4.0]	2.895	2.895 ± 0.004	2.757	2.758 ± 0.004
$\log(R^e_{\rm br}/{\rm MV})$	[3.0, 6.0]	3.698	3.691 ± 0.02	3.728	3.722 ± 0.015
$\log(m_\chi/{\rm GeV})$	[0.0, 7.0]	3.78	3.786 ± 0.12	2.936	2.954 ± 0.023
$\log(\langle\sigma v\rangle)$[b]	$[-28.0, -18.0]$	-21.72	-21.71 ± 0.2	-22.72	-22.69 ± 0.034
c_{e^+}	[0.25, 4.0]	2.934	2.942 ± 0.026	1.592	1.601 ± 0.016
ϕ/MV	[100, 1500]	1472.0	1475.0 ± 8.8	670.8	674.9 ± 8.7

[a]Postpropagated normalization flux of e^- at 25 GeV in units of $\rm cm^{-2}\,s^{-1}\,sr^{-1}\,MeV^{-1}$.
[b]In units of $\rm cm^3\,s^{-1}$.

Adopting the propagation parameters as the best-fitting values shown in Table I, we then constrain the injection parameters of Eq. (4) with the proton flux of AMS-02 [38]. The resulting nuclei injection parameters are given in Table II. Figure 2 shows the best-fitting results and the 95% confidence ranges of the proton fluxes, compared with the AMS-02 measurement.

The secondary production of electrons and positrons can then be calculated with the propagated proton (and helium) spectra. We use the parametrization presented in Ref. [61] to calculate the production spectrum of secondary electrons and positrons. To partially take into account the uncertainties when calculating the secondary fluxes, from, e.g., the proton-proton collision cross section, the enhancement

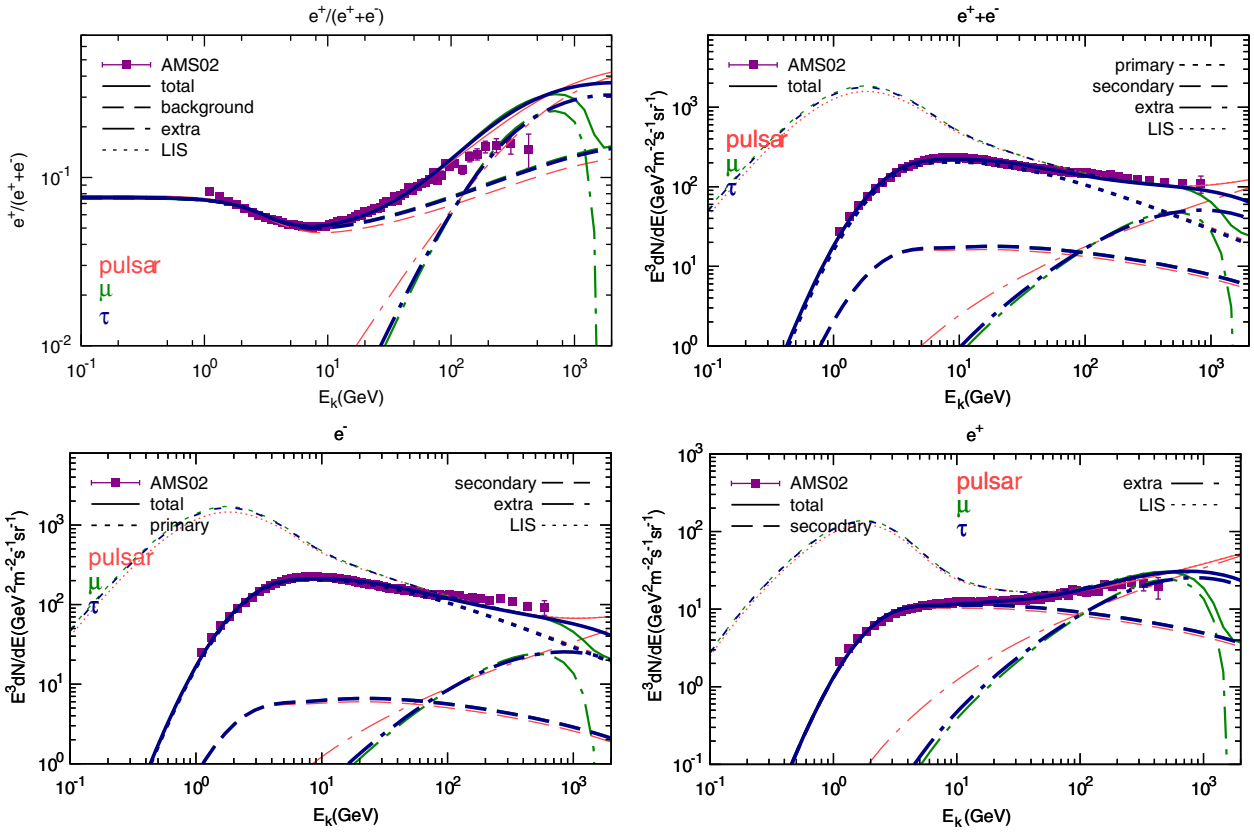

FIG. 3 (color online). The expected results for the best-fitting parameters in the DR scenario with one break of the primary electron injection spectrum. Top left: positron fraction $e^+/(e^+ + e^-)$; top right: electron plus positron flux $e^+ + e^-$; bottom left: electron flux e^-; and bottom right: positron flux e^+. The thin red, green, and thick blue curves represent the pulsar, DM annihilation into $\mu^+\mu^-$, and $\tau^+\tau^-$ final states, respectively. Different line styles represent different components as labeled.

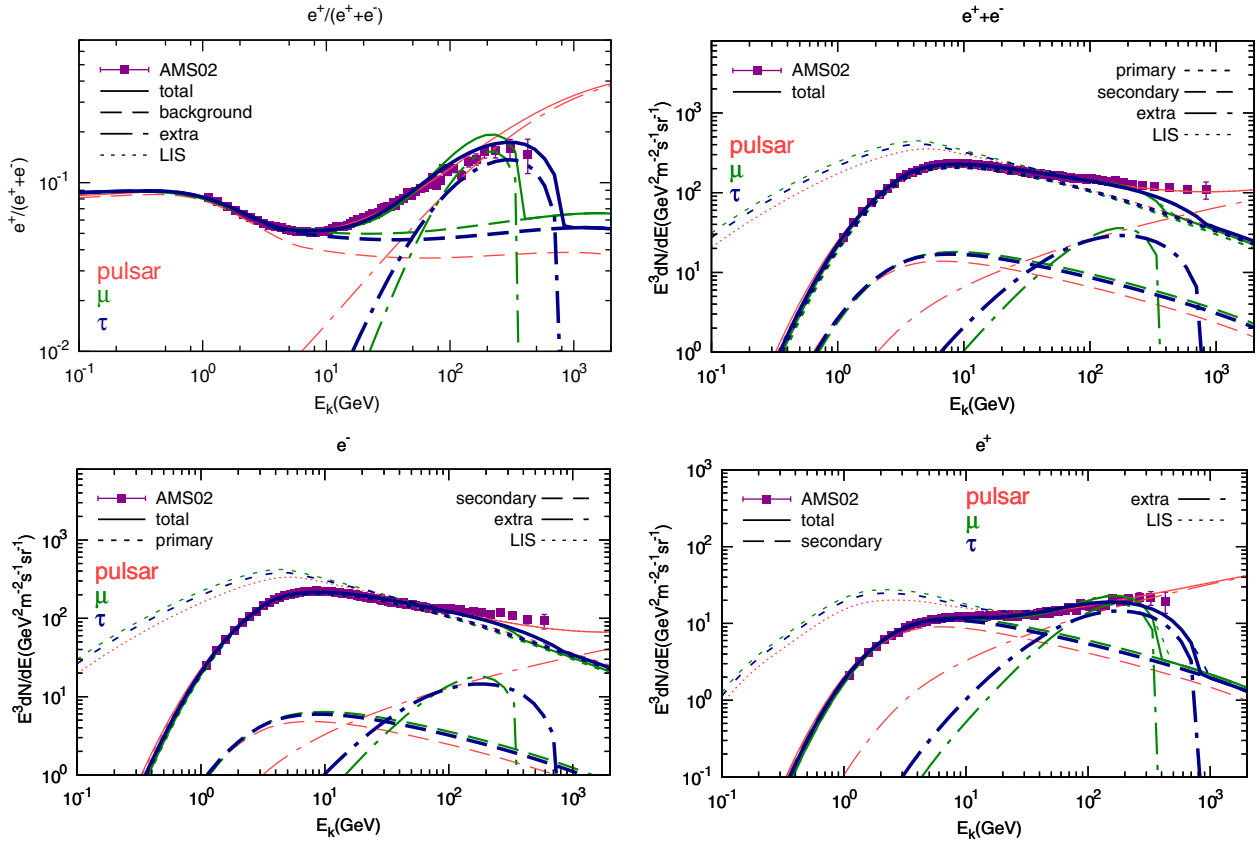

FIG. 4 (color online). Same as Fig. 3 but for the DC propagation scenario.

factor from heavier nuclei, and/or the propagation uncertainties, we employ a parameter c_{e^+} to rescale the calculated secondary flux to fit the data. Note that the above-mentioned uncertainties may not be simply represented with a constant factor, but most probably they are energy dependent [62,63]. Here, a constant factor is just an approximation, and the purpose is to fit the data.

About the primary electrons, we also assume a broken power-law form of the injection spectrum. Since electrons lose energies much more efficiently than the nuclei, the effect from recent and nearby sources may make the spectrum fluctuate significantly, especially at high energies [12]. Therefore, there might be more structures in the electron spectrum. We will discuss two cases in this work: one break case similar to Eq. (4) and a three-piece broken power law with two breaks. The latter is found to be required to fit the pre-AMS-02 lepton data [10,37,64,65]. Thus, the electron injection parameters are

$$\text{with one break}: (\gamma_1, \gamma_2, R^e_{\rm br}, A_e);$$
$$\text{with two breaks}: (\gamma_1, R^e_{\rm br}, \gamma_2, R^e_{\rm br2}, \gamma_3, A_e).$$

V. PARAMETERS FOR THE EXTRA SOURCES

In this paper, two kinds of extra sources, including pulsars and the DM annihilation, will be discussed. The pulsars are able to generate high-energy electron-positron

TABLE VI. Fitting χ^2 values and the contribution from each data. The number of data points for $e^+/(e^+ + e^-)$, $e^+ + e^-$, e^-, and e^+ are 63, 71, 70, and 69, respectively.

		Two breaks						One break					
		$\frac{\chi^2}{\text{d.o.f}}$	χ^2	$\frac{e^+}{e^+ + e^-}$	$e^+ + e^-$	e^-	e^+	$\frac{\chi^2}{\text{d.o.f}}$	χ^2	$\frac{e^+}{e^+ + e^-}$	$e^+ + e^-$	e^-	e^+
DR	Pulsar	1.1	287.1	48.57	99.02	60.03	79.45	2.75	725.2	132.7	271.8	211.7	109.0
	μ	1.12	293.4	40.7	113.8	61.0	77.95	3.01	797.9	242.4	245.5	206.9	103.1
	τ	1.11	291.0	42.62	106.4	63.38	78.6	2.94	779.9	213.9	252.2	209.9	103.9
DC	Pulsar	0.411	107.6	51.58	17.33	17.62	21.07	1.42	374.2	89.04	121.3	119.1	44.78
	μ	1.27	334.8	116.1	90.8	35.97	91.93	3.95	1048.0	484.1	250.0	179.8	134.1
	τ	0.575	151.1	65.0	30.18	17.97	37.91	2.4	636.5	168.5	228.1	165.1	74.84

pairs through the electromagnetic cascade in the magnetic pole region, which could cause the observed excess [15–19]. The injection spectrum of the electrons and positrons is usually assumed to be a power law with an exponential cutoff,

$$q_e^{\rm psr} = A_{\rm psr}(R/{\rm MV})^{-\alpha}\exp(-R/R_{\rm c}), \quad (5)$$

where $A_{\rm psr}$ is the normalization factor, α is the spectral index, and $R_{\rm c}$ is the cutoff rigidity. We adopt a continuous and stable pulsar injection. The spatial distribution obeys the same form of Eq. (3), with slightly different parameters $a = 2.35$ and $b = 5.56$ [66].

The particle and antiparticle of DM in the Galaxy, if the interaction is strong enough, can also annihilate with each other and produce standard model particles that are injected in the Galaxy as CRs. Since there is no obvious excess of antiprotons from the secondary expectation during the CR propagation compared with the data [67], leptonical annihilation final states are expected [25,26]. We therefore discuss the model with annihilation final states of a pair of muons or tauons. We use the results of PPPC 4 DM ID [68], which includes the electroweak corrections [69], to calculate the electron (positron) spectrum from DM annihilation. The Navarro–Frenk–White density profile [70]

$$\rho(r) = \frac{\rho_s}{(r/r_s)(1+r/r_s)^2}, \quad (6)$$

where $\rho_s = 20$ kpc and $\rho_s = 0.26$ GeV cm^{-3}, is adopted to describe the spatial distribution of DM in the Milky Way halo. The free parameters in the DM annihilation scenario include the DM particle mass m_χ and the velocity-weighted average annihilation cross section $\langle\sigma v\rangle$.

VI. FITTING RESULTS

The data sets used in this study include the latest measurements of the positron fraction $e^+/(e^+ + e^-)$,

TABLE VII. Fitting results of the pulsar model with two breaks in the e^- injection spectrum.

		DR		DC	
	Prior range	Best	Mean	Best	Mean
$\log(A_e)$[a]	[−10.5, −7.5]	−8.813	-8.812 ± 0.002	−8.896	-8.897 ± 0.002
γ_1	[1.0, 3.0]	1.302	1.361 ± 0.054	2.382	2.377 ± 0.022
$\log(R^e_{\rm br}/{\rm MV})$	[3.0, 5.0]	3.406	3.42 ± 0.02	3.881	3.873 ± 0.02
γ_2	[1.5, 4.0]	2.976	2.972 ± 0.005	2.836	2.829 ± 0.011
$\log(R^e_{\rm br2}/{\rm MV})$	[4.0, 6.0]	4.778	4.794 ± 0.028	4.717	4.747 ± 0.044
γ_3	[1.5, 4.0]	2.668	2.656 ± 0.02	2.586	2.571 ± 0.02
$\log(A_{\rm psr})$[b]	[−35.0, −20.0]	−28.88	-28.71 ± 0.59	−26.8	-26.77 ± 0.46
α	[1.0, 2.4]	1.185	1.221 ± 0.12	1.564	1.569 ± 0.096
$\log(R_{\rm c}/{\rm MeV})$	[4.0, 10.0]	5.853	5.923 ± 0.22	6.073	6.087 ± 0.23
c_{e^+}	[0.25, 4.0]	3.029	3.02 ± 0.025	1.53	1.512 ± 0.048
ϕ/MV	[100, 1500]	1499.0	1495.0 ± 4.4	672.8	667.3 ± 16.0

[a]Postpropagated normalization flux of e^- at 25 GeV in units of cm^{-2} s^{-1} sr^{-1} MeV^{-1}.
[b]Prepropagated normalization of pulsar injection at 1 MeV in units of cm^{-3} s^{-1} MeV^{-1}.

TABLE VIII. Fitting results of the DM annihilation scenario in the $\mu^+\mu^-$ channel with two breaks in the e^- injection spectrum.

		DR		DC	
	Prior range	Best	Mean	Best	Mean
$\log(A_e)$[a]	[−10.5, −7.5]	−8.813	-8.812 ± 0.001	−8.887	-8.888 ± 0.002
γ_1	[1.0, 3.0]	1.501	1.53 ± 0.028	2.427	2.427 ± 0.022
$\log(R^e_{\rm br}/{\rm MV})$	[3.0, 5.0]	3.473	3.48 ± 0.013	3.849	3.847 ± 0.016
γ_2	[1.5, 4.0]	2.976	2.971 ± 0.005	2.894	2.896 ± 0.01
$\log(R^e_{\rm br2}/{\rm MV})$	[4.0, 6.0]	4.787	4.803 ± 0.029	4.712	4.713 ± 0.038
γ_3	[1.5, 4.0]	2.654	2.647 ± 0.021	2.558	2.553 ± 0.023
$\log(m_\chi/{\rm GeV})$	[0.0, 7.0]	2.964	2.957 ± 0.049	2.621	2.621 ± 0.02
$\log(\langle\sigma v\rangle)$[b]	[−28.0, −18.0]	−23.3	-23.31 ± 0.085	−23.53	-23.53 ± 0.032
c_{e^+}	[0.25, 4.0]	3.053	3.049 ± 0.013	1.855	1.858 ± 0.015
ϕ/MV	[100, 1500]	1500.0	1498.0 ± 2.2	781.8	784.8 ± 8.2

[a]Postpropagated normalization flux of e^- at 25 GeV in units of cm^{-2} s^{-1} sr^{-1} MeV^{-1}.
[b]In units of cm^3 s^{-1}.

TABLE IX. Fitting results of the DM annihilation scenario in the $\tau^+\tau^-$ channel with two breaks in the e^- injection spectrum.

		DR		DC	
	Prior range	Best	Mean	Best	Mean
$\log(A_e)$[a]	$[-10.5, -7.5]$	-8.813	-8.812 ± 0.002	-8.891	-8.891 ± 0.002
γ_1	[1.0, 3.0]	1.502	1.528 ± 0.025	2.409	2.402 ± 0.021
$\log(R^e_{\rm br}/{\rm MV})$	[3.0, 5.0]	3.471	3.48 ± 0.012	3.842	3.84 ± 0.015
γ_2	[1.5, 4.0]	2.972	2.969 ± 0.005	2.855	2.856 ± 0.009
$\log(R^e_{\rm br2}/{\rm MV})$	[4.0, 6.0]	4.789	4.803 ± 0.029	4.756	4.746 ± 0.04
γ_3	[1.5, 4.0]	2.656	2.651 ± 0.021	2.548	2.555 ± 0.021
$\log(m_\chi/{\rm GeV})$	[0.0, 7.0]	3.59	3.581 ± 0.081	3.003	3.006 ± 0.028
$\log(\langle\sigma v\rangle)$[b]	$[-28.0, -18.0]$	-22.13	-22.14 ± 0.14	-22.68	-22.67 ± 0.039
c_{e^+}	[0.25, 4.0]	3.035	3.027 ± 0.015	1.719	1.727 ± 0.018
ϕ/MV	[100, 1500]	1500.0	1496.0 ± 3.1	728.9	732.6 ± 9.3

[a]Postpropagated normalization flux of e^- at 25 GeV in units of $\rm cm^{-2}\,s^{-1}\,sr^{-1}\,MeV^{-1}$.
[b]In units of$\rm cm^3\,s^{-1}$.

fluxes of e^-, e^+, and $(e^+ + e^-)$ by AMS-02 [39–41]. These data may not be fully uncorrelated, since the positron fraction may be derived from the fluxes of e^- and e^+. However, the analysis methods are different for various kinds of measurements, and the systematic uncertainties also differ from one another. Therefore, we adopted all these data in the study, though the statistics of the data would be overestimated. We have also tested that when dropping one group of the data the results are almost unchanged. We further select the data above 1 GeV, since the lowest-energy data may be significantly affected by the solar modulation and may not be well modeled in the force-field approximation [57]. The spectral index of electrons/positrons injected by pulsars, and possibly altered by the surrounding pulsar wind nebulae, is actually very uncertain. In this work, we limit α to the range between 1.0 and 2.4, according to the radio and γ-ray observations of pulsars [71–73].

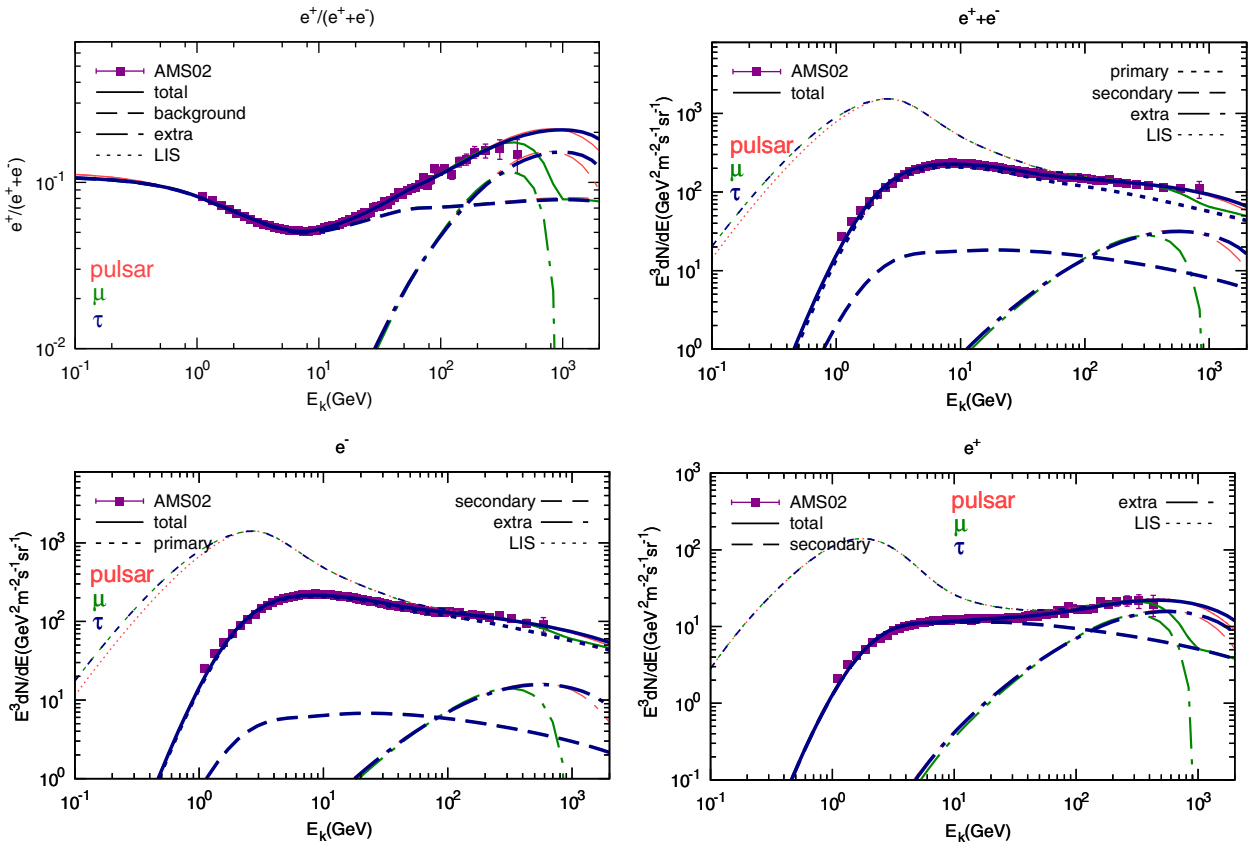

FIG. 5 (color online). The same as Fig. 3 but for the background model with two breaks in the electron injection spectrum.

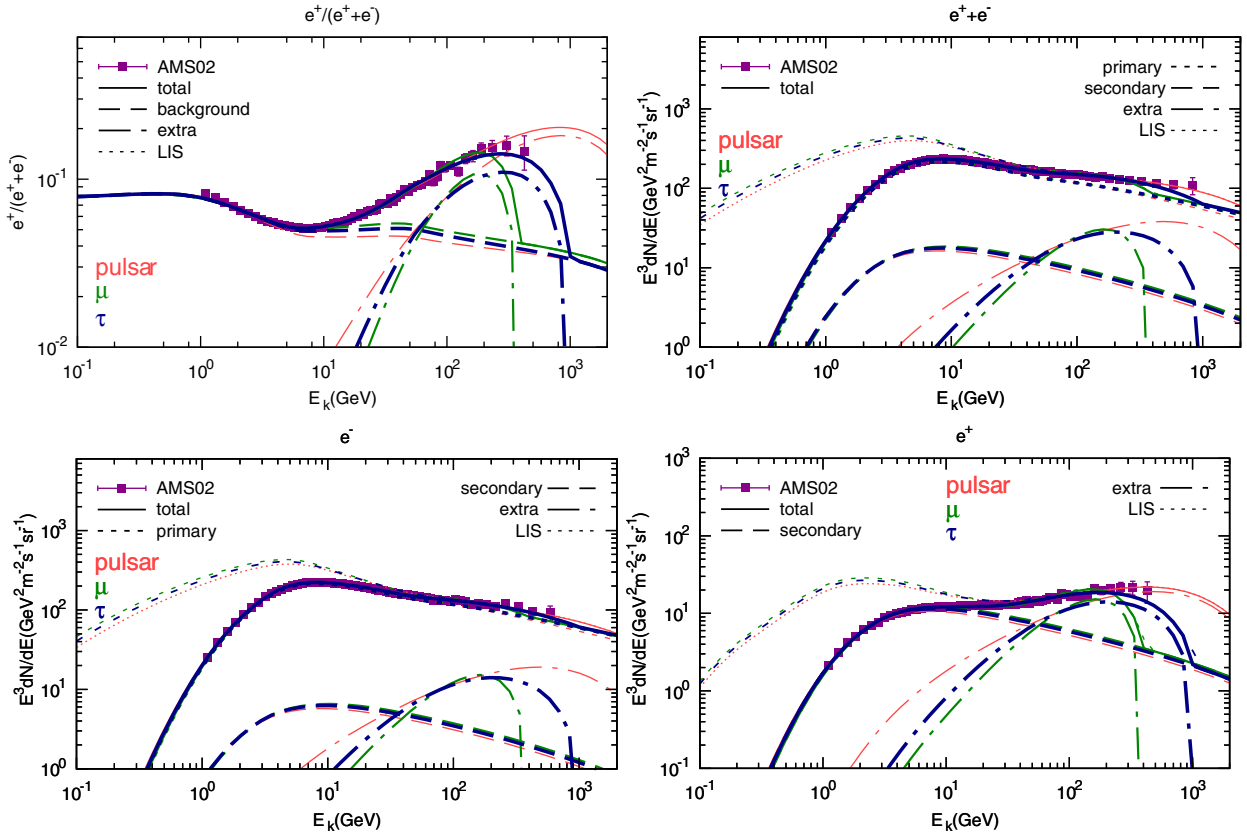

FIG. 6 (color online). The same as Fig. 5 but for the DC propagation scenario.

A. One break in primary electron spectrum

In this case, there are four parameters of the primary electrons. Together with c_{e^+}, ϕ and the extra source parameters, we have in total nine (eight) parameters for the pulsar (DM) scenario. The best-fitting parameters and the mean values as well as 1σ confidence ranges are shown in Tables III, IV, and V for the pulsar, DM annihilation into $\mu^+\mu^-$, and DM annihilation into $\tau^+\tau^-$, respectively. Figures 3 and 4 illustrate the comparison of the best-fitting results with the data, for DR and DC propagation scenarios. Table VI summarizes the fitting χ^2 values for each data set.

The results show not good enough fittings to data. From Figs. 3 and 4, it can be seen that, while the model may overproduce the positron fraction, it is not enough to reproduce the electron flux at high energies. This is similar to that we found before using the electron data from PAMELA/Fermi-LAT [9]. The fitting χ^2 values also show this issue. The minimum χ^2 value for these six fittings is 374.2, and the reduced χ^2 is about 1.42 for 264 degrees of freedom (d.o.f.). It corresponds to a 4.4σ deviation from a good fitting as expected.

Given the fittings are poor, the constraints on the model parameters by minimizing the χ^2 may not be physically meaningful. The pulsar model gives better fitting than the DM scenario, since the spectral index of electrons/positrons injected by the pulsar is enabled to vary and it has larger d.o.f. compared with the spectrum expected from DM annihilation. We further note that the χ^2 contributed from the e^- flux and the $e^+ + e^-$ flux are about two times larger than those from the e^+ flux, although the numbers of data points are comparable. It could be due to the fact that electrons have much higher statistics compared with the positrons. The failure to reproduce the high-energy electron spectrum well would result in a large χ^2 value. Therefore, we may need to change the background model to improve the fitting of the high-energy electron spectrum.

B. Two breaks in primary electron spectrum

A direct way to alleviate the tension shown above is to add more electrons at high energies, such as a spectral hardening [10,64,65]. For the nuclei spectra, similar spectral hardening above several hundred GV has been observed by ATIC [74], CREAM [75], and PAMELA [76] and could be naturally expected if there is a diversity of the source parameters [77]. Therefore, we apply a second break on the injection spectrum of the primary electrons characterized by two additional parameters γ_3 and $R^e_{\rm br2}$. The fitting results are shown in Tables VII, VIII, and IX and Figs. 5 and 6, respectively. We also show in Figs. 7 and 8 the derived one- and two-dimensional posterior

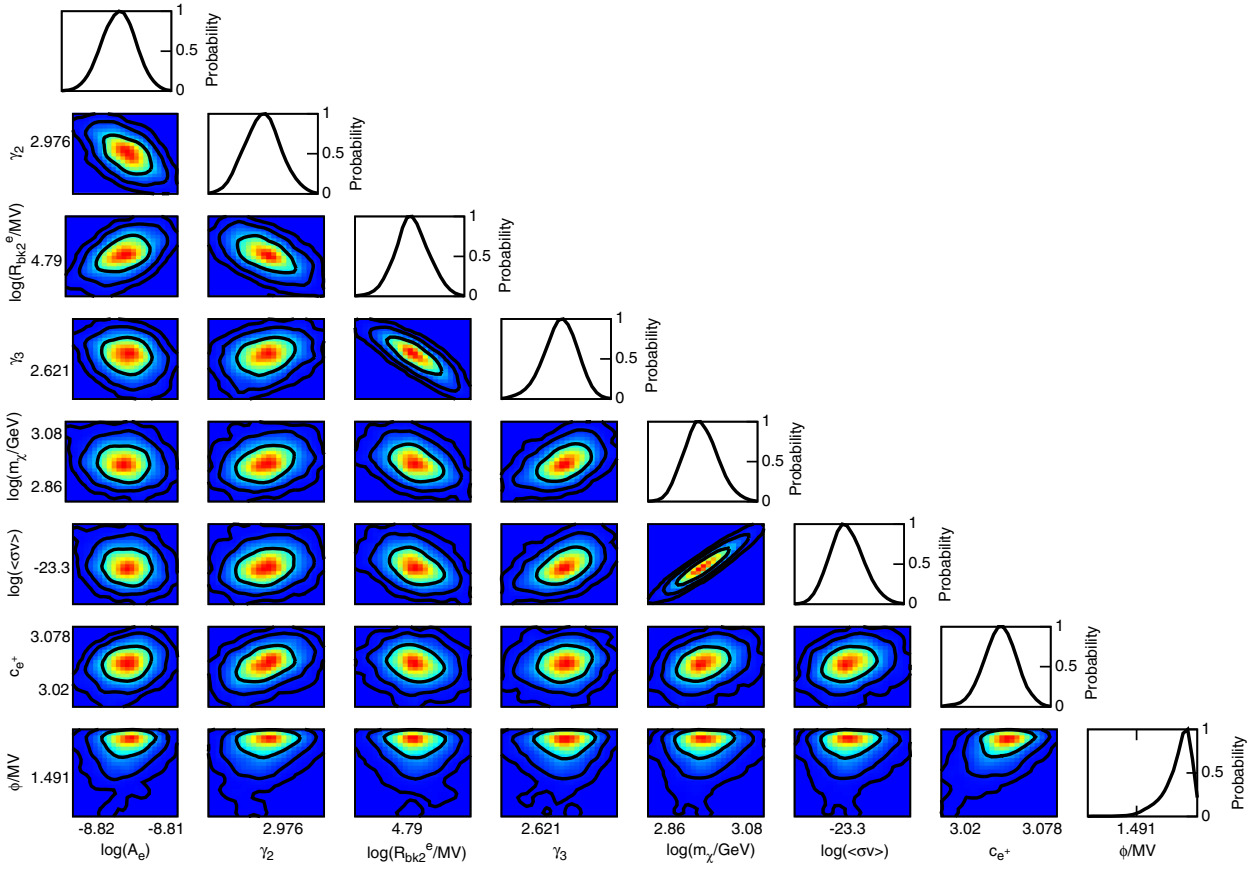

FIG. 7 (color online). The one- and two-dimensional distributions of part of the parameters for DM annihilation into the $\mu^+\mu^-$ channel. The background electrons have two breaks, and the propagation model is DR. The contours in the two-dimensional plots denote the 68.3%, 95.5%, and 99.7% confidence levels from inside to outside.

distributions of the most relevant parameters, choosing the DM annihilation into the μ channel as benchmark cases.

Significant improvements of the fittings can be seen from these results. It is shown from Table VI that in all the cases the reduced χ^2 values are about two times smaller than the previous case with one break. For most cases, the reduced χ^2 is close to or smaller than 1. Since the systematic errors are added quadratically to the statistical errors to calculate the χ^2, it is expected that the reduced χ^2 value will be smaller than 1 if the model does fit the data well (see, e.g., the minimum model of Ref. [40]). It can be seen from Figs. 5 and 6 that the contribution of positrons from the extra source dominates over the secondary component above ~50–100 GeV. For electrons, however, the background component will always dominate in the energy range from 1 GeV to 1 TeV.

We further find that the pulsar model and DM annihilation into $\tau^+\tau^-$ give comparable fittings to the data. However, the case for the $\mu^+\mu^-$ channel seems to be more complicated. In the DR scenario, it gives comparable fittings compared with the pulsar model and the DM annihilation into $\tau^+\tau^-$ channel, while in the DC scenario, the fitting results become worse. Figure 9 shows the comparison of the positron fluxes between DR and DC scenarios, for DM annihilation into the $\mu^+\mu^-$ channel. The reason for such a result might be the difference of the secondary positron spectrum in the two scenarios. As can be seen from Fig. 9, the secondary positron spectrum is softer in the DC scenario. This should be due to the fact that the DC model has a larger propagation parameter δ than the DR model. Since the positron spectrum from muon decay is very hard, a smaller value of DM mass is needed to better fit the data. It results in the failure to reproduce the high-energy tail of the positron spectrum. The positron spectrum from pulsar or tauon decay can be softer and thus can fit the data better than the muon model.[2]

VII. DISCUSSION

In this paper, we try to give a quantitative study on the AMS-02 results of the electron/positron fluxes. Although the AMS-02 data are precise enough, there are large uncertainties from the theoretical model parameters, such

[2]A four-muon final state may give better fitting to the AMS-02 data.

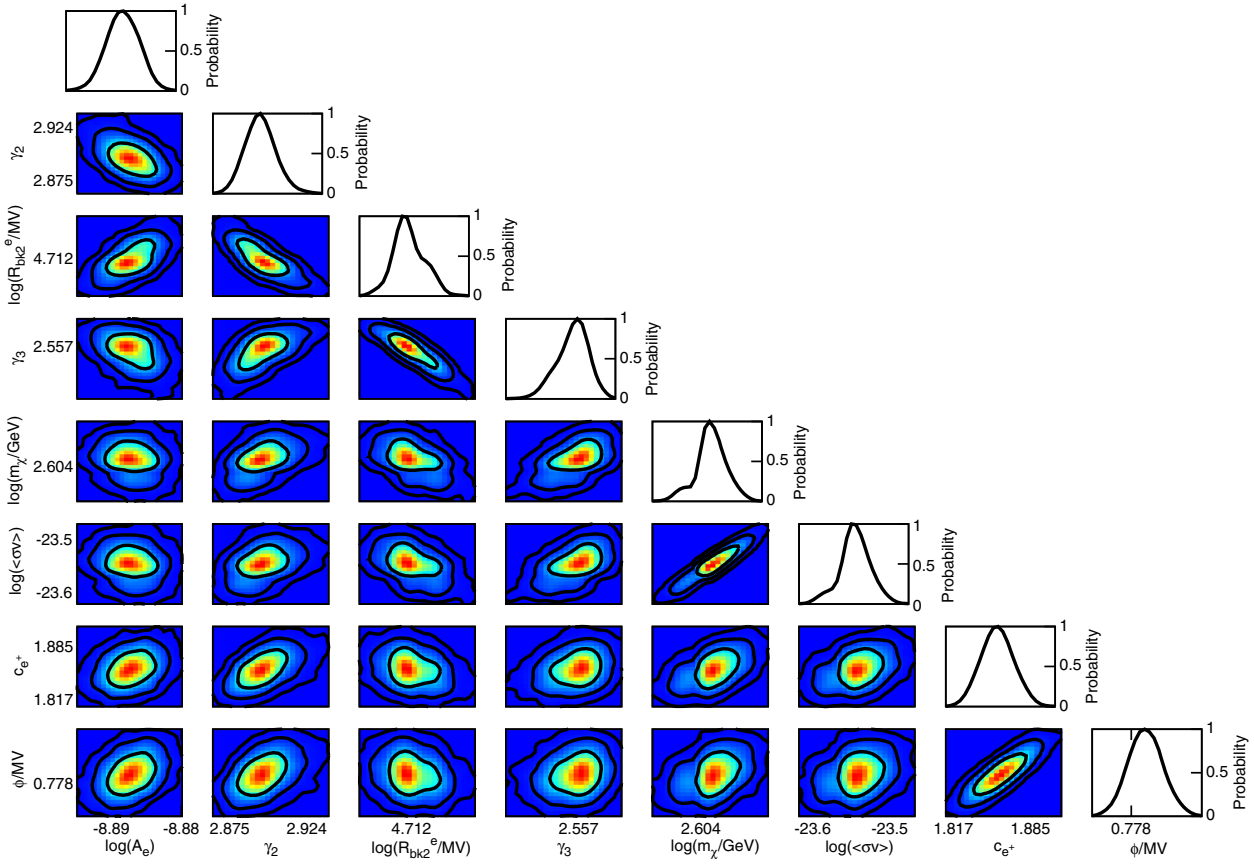

FIG. 8 (color online). The same as Fig. 7 but for the DC propagation scenario.

as the uncertainties from the CR propagation model, the treatment of the solar modulation, the Galactic gas distribution, and so on. In Ref. [37], we studied quite a few of such kinds of uncertainties as possible systematical uncertainties, including the propagation, the solar modulation and low-energy data selection, the hadronic interaction model, and so on. The study shows that, although the uncertainties of the model inputs seem to be large, the fitting results about the extra sources are under good control.

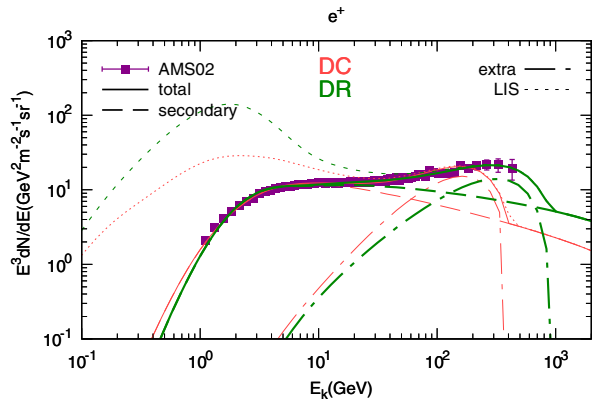

FIG. 9 (color online). Comparison of the positron spectra between the DC scenario (thin red) and DR scenario (green) with an extra source component from DM annihilation into the $\mu^+\mu^-$ final state.

As an illustration, we plot the 1σ and 2σ contours on the $m_\chi - \langle\sigma v\rangle$ parameter plane to show the uncertainties of the parameter determination for the scenarios discussed in this work. The solid (dashed) ones are for the case with two (one) breaks of the primary electron injection spectrum. The red ones are for DR propagation model, and the blues ones are for the DC model. The results do show some differences between DR and DC propagation models. Nevertheless, the shift of the central values as well as the contours is about a factor of 4, which is larger than that found in Ref. [37]. One possible reason for this difference might be that we do not include the HESS data at higher energies in this study. The HESS data, although they have large systematic uncertainties, should be useful to constrain the very high-energy behavior of the electron/positron spectra. The future experiments such as DAMPE[3] and HERD [78] may provide better measurements of the electron/positron spectra above TeV.

A main result of our fitting is that a new feature at the primary electron spectrum is strongly favored. Such a

[3]http://dpnc.unige.ch/dampe/

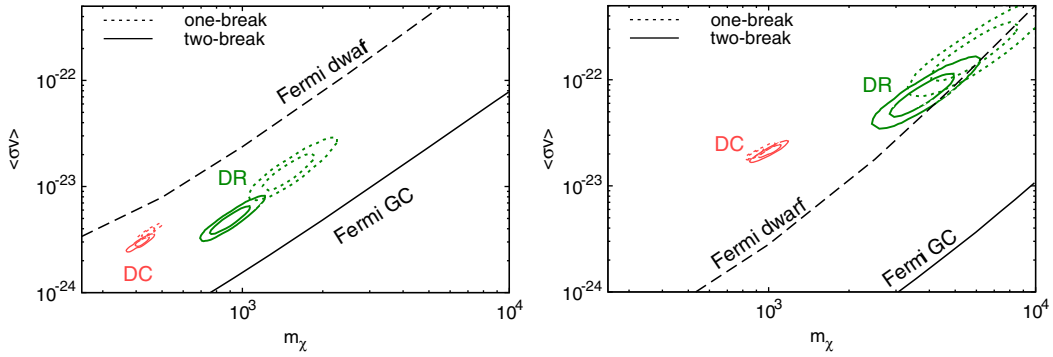

FIG. 10 (color online). 1σ and 2σ confidence regions in the $m_\chi - \langle\sigma v\rangle$ plane, together with the exclusion lines from Fermi γ-ray observations [83,84]. The left panel is for the μ channel, while the right panel is for the τ channel. Thin red contours are for DC scenario, and green ones are for the DR scenario. The dashed regions are for the case with only one break in the primary electron injection spectrum, while the solid regions are for those with an additional break.

feature indicates that the nearby and/or fresh CR sources may contribute to the high-energy electrons with a harder spectrum than the background [12]. Considering the large fluctuation of the electron/positron fluxes in space due to fast energy losses, it is quite reasonable that the high-energy electrons are dominated by the local sources. One possible signature of such a scenario may be the fine structures of the electron/positron spectra, which may be investigated with future observations [79]. Another possible probe of the local sources could be the anisotropy measurements of the electrons [80].

Another interesting conclusion of this study is that in general the DC model is more favored than the DR model by the lepton spectra (Table VI). The DM model with the $\mu^+\mu^-$ channel is an exception that we have discussed above. The reason is that the local interstellar spectrum has a bump at low energy in the DR model due to the reacceleration, and thus a large solar modulation potential has to be introduced to suppress the bump to fit the data. Such a bump is necessary to better fit the B/C ratio data [56], especially the HEAO data [81]. However, the AMS-02 data about the B/C ratio do not strongly favor a bump, and hence the reacceleration for $E_k \lesssim 1$ GeV/nucleon [38]. The current data about the B/C ratio by AMS-02 is not able to distinguish the DR from the DC model. Therefore, to finally address the question of whether the reacceleration is favored, one needs a more precise measurement of the B/C ratio down to sub-GeV. A similar conclusion has also been obtained in the study of the synchrotron radiation [82]. It was found that the DR model predicted higher radio emission than observed.

Finally, it is well known that the DM annihilation scenario of the positron excess is strongly constrained by the γ-ray observation. The exclusion limit derived from γ-ray observations of the dwarf galaxies by Fermi [83] and the Galactic center [84] are shown in Fig. 10. Similar to the conclusion in Ref. [9], the constraints from the Galactic center observation excludes all the DM scenarios. But these results suffer from large uncertainty of the small-scale DM density profile. The constraints from the dwarf galaxies are much more solid. The DM annihilation to the τ channel shows tension with the γ-ray observations. For the μ channel, the current γ-ray data from the dwarf galaxies is still not able to exclude the required parameter region to explain the lepton excess.

VIII. CONCLUSIONS

In this paper, we give a global fitting to the AMS-02 new results of the positron fraction, electron plus positron, electron, and positron spectra to determine the primary electron spectrum as well as the extra e^+e^- sources such as pulsars or DM. Two typical CR propagation models, the DR and DC models, are discussed.

We find that, in order to fit the data, an additional break (hardening) at the primary electron spectrum at ~60 GeV is necessary. With such a primary electron spectrum, both the pulsar scenario and the DM scenario can give a good fit to the data, with χ^2/d.o.f. close to or smaller than 1. The fittings are too poor to be acceptable without the additional hardening of the primary spectrum. The best case without the additional break is the DC scenario with pulsars as the extra source, which gives $\chi^2/\text{d.o.f.} = 374.2/264$ and corresponds to a 4.4σ deviation from expectation.

In the two-break electron background case, both the pulsar and DM model can give good fittings to the AMS-02 lepton data. If DM annihilates into the μ final state, the fitting value of its mass is about 0.4–1.5 TeV, and the annihilation cross section is about $(3-10)\times 10^{-24}\ \text{cm}^3\,\text{s}^{-1}$. For the τ final state, the DM mass is about 1–7 TeV, and the cross section is about $(2-20)\times 10^{-23}\ \text{cm}^3\,\text{s}^{-1}$. It is interesting to note that the DM scenario can reproduce the potential drop of the positron fraction data at ~300 GeV with the best-fitting mass values.

We further find that to fit the lepton data the DC propagation model is more favorable than the DR model. This is because the DR model will induce a bump at the local interstellar spectrum as a consequence of reacceleration. Such a bump is favored by the HEAO B/C ratio data but is not favored by the lepton spectra. Therefore, it is very important for the AMS-02 to give an independent measurement of the B/C ratio down to sub-GeV so as to determine the propagation model.

ACKNOWLEDGMENTS

We thank Z.-H. Li, Z.-C. Tang, Z.-L. Weng, and W.-W. Xu for helpful discussions. This work is supported by the National Natural Science Foundation of China (NSFC) under Grants No. 11475191 and No. 11135009 and by the Strategic Priority Research Program "The Emergence of Cosmological Structures" of the Chinese Academy of Sciences, under Grant No. XDB09000000.

[1] O. Adriani *et al.* (PAMELA Collaboration), Nature (London) **458**, 607 (2009).
[2] O. Adriani *et al.* (PAMELA Collaboration), Phys. Rev. Lett. **106**, 201101 (2011).
[3] A. A. Abdo *et al.* (Fermi LAT Collaboration), Phys. Rev. Lett. **102**, 181101 (2009).
[4] M. Ackermann *et al.* (Fermi LAT Collaboration), Phys. Rev. D **82**, 092004 (2010).
[5] J. Chang *et al.*, Nature (London) **456**, 362 (2008).
[6] F. Aharonian *et al.* (H.E.S.S. Collaboration), Phys. Rev. Lett. **101**, 261104 (2008).
[7] D. B. Tridon, P. Colin, L. Cossio, M. Doro, and V. Scalzotto (MAGIC Collaboration), arXiv:1110.4008.
[8] M. Aguilar *et al.* (AMS Collaboration), Phys. Rev. Lett. **110**, 141102 (2013).
[9] Q. Yuan, X.-J. Bi, G.-M. Chen, Y.-Q. Guo, S.-J. Lin, and X. Zhang, Astropart. Phys. **60**, 1 (2015).
[10] L. Feng, R.-Z. Yang, H.-N. He, T.-K. Dong, Y.-Z. Fan, and J. Chang, Phys. Lett. B **728**, 250 (2014).
[11] H.-B. Jin, Y.-L. Wu, and Y.-F. Zhou, J. Cosmol. Astropart. Phys. 11 (2013) 026.
[12] M. Di Mauro, F. Donato, N. Fornengo, R. Lineros, and A. Vittino, J. Cosmol. Astropart. Phys. 04 (2014) 006.
[13] S. Barwick *et al.* (HEAT Collaboration), Astrophys. J. **482**, L191 (1997).
[14] M. Aguilar *et al.* (AMS-01 Collaboration), Phys. Lett. B **646**, 145 (2007).
[15] C. S. Shen, Astrophys. J. Lett. **162**, L181 (1970).
[16] L. Zhang and K. S. Cheng, Astron. Astrophys. **368**, 1063 (2001).
[17] H. Yuksel, M. D. Kistler, and T. Stanev, Phys. Rev. Lett. **103**, 051101 (2009).
[18] D. Hooper, P. Blasi, and P. D. Serpico, J. Cosmol. Astropart. Phys. 01 (2009) 025.
[19] S. Profumo, Central Eur. J. Phys. **10**, 1 (2012).
[20] P. Blasi, Phys. Rev. Lett. **103**, 051104 (2009).
[21] H.-B. Hu, Q. Yuan, B. Wang, C. Fan, J.-L. Zhang, and X.-J. Bi, Astrophys. J. **700**, L170 (2009).
[22] Y. Fujita, K. Kohri, R. Yamazaki, and K. Ioka, Phys. Rev. D **80**, 063003 (2009).
[23] L. Bergstrom, T. Bringmann, and J. Edsjo, Phys. Rev. D **78**, 103520 (2008).
[24] V. Barger, W. Y. Keung, D. Marfatia, and G. Shaughnessy, Phys. Lett. B **672**, 141 (2009).
[25] M. Cirelli, M. Kadastik, M. Raidal, and A. Strumia, Nucl. Phys. **B813**, 1 (2009).
[26] P.-f. Yin, Q. Yuan, J. Liu, J. Zhang, X.-j. Bi, S.-h. Zhu, and X. Zhang, Phys. Rev. D **79**, 023512 (2009).
[27] J. Zhang, X.-J. Bi, J. Liu, S.-M. Liu, P.-F. Yin, Q. Yuan, and S.-H. Zhu, Phys. Rev. D **80**, 023007 (2009).
[28] L. Bergstrom, J. Edsjo, and G. Zaharijas, Phys. Rev. Lett. **103**, 031103 (2009).
[29] X.-G. He, Mod. Phys. Lett. A **24**, 2139 (2009).
[30] Y.-Z. Fan, B. Zhang, and J. Chang, Int. J. Mod. Phys. D **19**, 2011 (2010).
[31] P. D. Serpico, Astropart. Phys. **39–40**, 2 (2012).
[32] M. Cirelli, Pramana **79**, 1021 (2012).
[33] X.-J. Bi, P.-F. Yin, and Q. Yuan, Front. Phys. China **8**, 794 (2013).
[34] A. Lewis and S. Bridle, Phys. Rev. D **66**, 103511 (2002).
[35] J. Liu, Q. Yuan, X. Bi, H. Li, and X. Zhang, Phys. Rev. D **81**, 023516 (2010).
[36] J. Liu, Q. Yuan, X.-J. Bi, H. Li, and X. Zhang, Phys. Rev. D **85**, 043507 (2012).
[37] Q. Yuan and X.-J. Bi, arXiv:1408.2424.
[38] AMS-02 Collaboration, International Cosmic Ray Conference, Rio de Janeiro, Brazil, 2013 (unpublished), http://www.ams02.org/2013/07/new-results-from-ams-presented-at-icrc-2013.
[39] L. Accardo *et al.* (AMS Collaboration), Phys. Rev. Lett. **113**, 121101 (2014).
[40] M. Aguilar *et al.* (AMS Collaboration), Phys. Rev. Lett. **113**, 121102 (2014).
[41] M. Aguilar *et al.* (AMS Collaboration), Phys. Rev. Lett. **113**, 221102 (2014).
[42] V. S. Berezinskii, S. V. Bulanov, V. A. Dogiel, and V. S. Ptuskin, *Astrophysics of Cosmic Rays*, edited by V. L. Ginzburg (North-Holland, Amsterdam, 1990).
[43] E. S. Seo and V. S. Ptuskin, Astrophys. J. **431**, 705 (1994).
[44] A. Strong and I. Moskalenko, Astrophys. J. **509**, 212 (1998).
[45] I. Moskalenko and A. Strong, Astrophys. J. **493**, 694 (1998).
[46] R. A. Mewaldt, J. R. Jokipii, M. A. Lee, E. Möbius, and T. H. Zurbuchen, eds., *Acceleration and Transport of Energetic Particles Observed in the Heliosphere.*, American Institute of Physics Conference Series (American Institute of Physics, New York, 2000), Vol. 528.
[47] N. E. Yanasak *et al.*, Astrophys. J. **563**, 768 (2001).

[48] F. A. Hagen, A. J. Fisher, and J. F. Ormes, Astrophys. J. **212**, 262 (1977).
[49] A. Buffington, C. D. Orth, and T. S. Mast, Astrophys. J. **226**, 355 (1978).
[50] W. R. Webber and J. Kish, in *International Cosmic Ray Conference, 1979*, Vol. 1, p. 389, http://adsabs.harvard.edu/abs/1979ICRC....1..389W.
[51] M. Garcia-Munoz, J. A. Simpson, and J. P. Wefel, International Cosmic Ray Conference, 1981, Vol. **2**, p. 72.
[52] J. A. Simpson and M. Garcia-Munoz, *Space Sci. Rev.* 46, 205 (1988).
[53] T. Hams *et al.*, Astrophys. J. **611**, 892 (2004).
[54] J. J. Connell, Astrophys. J. Lett. **501**, L59 (1998).
[55] A. Lukasiak, *International Cosmic Ray Conference, 1999*, Vol. 3, p. 41.
[56] I. V. Moskalenko, A. W. Strong, J. F. Ormes, and M. S. Potgieter, Astrophys. J. **565**, 280 (2002).
[57] L. Gleeson and W. Axford, Astrophys. J. **154**, 1011 (1968).
[58] A. W. Strong, I. V. Moskalenko, and V. S. Ptuskin, Annu. Rev. Nucl. Part. Sci. **57**, 285 (2007).
[59] M. Ackermann *et al.*, Astrophys. J. **750**, 3 (2012).
[60] R. Trotta, G. Jóhannesson, I. V. Moskalenko, T. A. Porter, R. R. de Austri, and A. W. Strong, Astrophys. J. **729**, 106 (2011).
[61] T. Kamae, N. Karlsson, T. Mizuno, T. Abe, and T. Koi, Astrophys. J. **647**, 692 (2006).
[62] T. Delahaye, R. Lineros, F. Donato, N. Fornengo, J. Lavalle, P. Salati, and R. Taillet, Astron. Astrophys. **501**, 821 (2009).
[63] M. Mori, Astropart. Phys. **31**, 341 (2009).
[64] Q. Yuan and X.-J. Bi, Phys. Lett. B **727**, 1 (2013).
[65] I. Cholis and D. Hooper, Phys. Rev. D **88**, 023013 (2013).
[66] D. R. Lorimer, *Young Neutron Stars and Their Environments*, edited by F. Camilo and B. M. Gaensler, International Astronomical Union (IAU) Symposium Vol. 218 (American Scientific Publishers, Sydney, 2003), p. 105.
[67] O. Adriani *et al.* (PAMELA Collaboration), Phys. Rev. Lett. **105**, 121101 (2010).
[68] M. Cirelli, G. Corcella, A. Hektor, G. Hütsi, M. Kadastik, P. Panci, M. Raidal, F. Sala, and A. Strumia, J. Cosmol. Astropart. Phys. 03 (2011) 051.
[69] P. Ciafaloni, D. Comelli, A. Riotto, F. Sala, A. Strumia, and A. Urbano, J. Cosmol. Astropart. Phys. 03 (2011) 019.
[70] J. F. Navarro, C. S. Frenk, and S. D. White, Astrophys. J. **490**, 493 (1997).
[71] S. P. Reynolds, Astrophys. J. **327**, 853 (1988).
[72] D. Thompson *et al.*, Astrophys. J. **436**, 229 (1994).
[73] J. Fierro *et al.*, Astrophys. J. **447**, 807 (1995).
[74] A. D. Panov *et al.*, Bull. Russ. Acad. Sci. Phys. **71**, 494 (2007).
[75] H. Ahn *et al.*, Astrophys. J. **714**, L89 (2010).
[76] O. Adriani *et al.* (PAMELA Collaboration), Science **332**, 69 (2011).
[77] Q. Yuan, B. Zhang, and X.-J. Bi, Phys. Rev. D **84**, 043002 (2011).
[78] S. Zhang (the HERD collaboration), arXiv:1407.4866.
[79] P.-F. Yin, Z.-H. Yu, Q. Yuan, and X.-J. Bi, Phys. Rev. D **88**, 023001 (2013).
[80] T. Linden and S. Profumo, Astrophys. J. **772**, 18 (2013).
[81] J. J. Engelmann, P. Ferrando, A. Soutoul, P. Goret, and E. Juliusson, Astron. Astrophys. **233**, 96 (1990).
[82] A. Strong, E. Orlando, and T. Jaffe, Astron. Astrophys. **534**, A54 (2011).
[83] M. Ackermann *et al.* (Fermi-LAT Collaboration), Phys. Rev. D **89**, 042001 (2014).
[84] X. Huang, Q. Yuan, P.-F. Yin, X.-J. Bi, and X. Chen, J. Cosmol. Astropart. Phys. 11 (2012) 048.